Flowfield Measurements in an Unstable Ramjet Burner

D. M. Reuter,* U. G. Hegde,† and B. T. Zinn‡
Georgia Institute of Technology, Atlanta, Georgia 30332

This paper describes the flowfield in the flame region of an unstable laboratory ramjet burner. The steady and unsteady components of the velocity field are obtained using a conditional sampling laser-Doppler velocimetry technique. The vorticity field is also derived from the measured velocity field. It is shown that combustion instability in the ramjet burner is accompanied by unsteady vortex shedding at the flame holding region. The vortex shedding occurs at the frequency of instability, and it periodically distorts the flame front causing a cyclic variation of the flame area. This variation in the flame area results in a strong unsteady heat release rate capable of driving the longitudinal instabilities in the system.

Introduction

COMBUSTION instabilities often occur in coaxial, dump-type ramjet combustors. These instabilities are characterized by either low-frequency (i.e., rumble) or high-frequency (i.e., screech) pressure and velocity oscillations. The low-frequency pressure and velocity oscillations are encountered in the range of 50–500 Hz and involve longitudinal acoustic oscillations at a natural frequency of the combustor. These oscillations are undesirable because their interaction with the inlet shock system of the ramjet may result in inlet unstarting and loss of engine performance. In addition, excessive vibrational loads on the system may result. This paper investigates the mechanisms controlling the low-frequency instability by studying the flowfield in the combustion zone of a laboratory ramjet burner.

Previous studies[1-7] of this problem have suggested that these low-frequency instabilities are driven by unsteady combustion in vortical structures shed at the flame holding region in the ramjet combustor. Unstable modes of the shear layer formed in the wake of the flame holder are believed to interact with the unstable acoustic mode of the combustor at the frequency of instability to give rise to the vortex shedding process. This paper describes further investigations of this problem and presents results of experimental measurements that provide a detailed description of the velocity field in the ramjet flame region as well as yields insights into the vortex shedding process. The measurements also show that the shed vortices affect the flame structure and cause an oscillatory heat release rate capable of sustaining the acoustic instability.

The following Experimental Setup section briefly describes the ramjet simulator specifically developed for this investigation and the velocity measurement technique. The Experimental Results section presents measurements of the unsteady velocity and the shear layer structure and provides details of the vortex shedding process. The effects of the unsteady vortex structures on the ramjet flame are also discussed.

Experimental Setup

A schematic diagram of the experimental apparatus, described in detail in earlier papers,[1,2] is shown in Fig. 1. It consists of a 3-m long, 7.5 × 5 cm^2 rectangular duct, which has an inlet, combustor, and exhaust sections. A combustible mixture of propane and air is introduced into the inlet through a sintered stainless steel injector. A W-shaped premixed flame (see Fig. 2) is stabilized in the combustor section by means of two, 6-mm diam, steel cylinders, which are held in position perpendicular to the flame by two thin support wires. Figure 2, which is drawn to scale, shows the geometry of the flame arrangement. This configuration results in strong acoustic oscillations of the order of 140 dB at the first natural longitudinal frequency f_0 of the duct and is therefore appropriate for investigating the instability mechanisms. The side walls of the combustor section are made of quartz to enable optical access to the flame region. In addition, pressure transducers and thermocouples are used to characterize the acoustic pressure field and the temperature rise across the flame.

The flow entering the combustion chamber is parallel and uniform. The cold flow velocity is 1.9 m/s, resulting in a Reynolds number, based on the duct height, of the order of 10,000. Any residual turbulence or large-scale velocity fluctuations in the inlet section of the duct are suppressed at the entrance of the combustor by means of a 63-mm-long honeycomb section, which suppresses the measured turbulence to 2% of the freestream velocity. A low freestream turbulence level is important because large random velocity fluctuations may mask the periodic velocity changes associated with the instability.

Velocity measurements have been obtained using laser-Doppler velocimetry (LDV). The LDV system used in the present investigation has been installed in the two-component, dual-beam arrangement, operates in the forward-scatter mode, and provides measurements of the axial and normal velocities. Both channels of the LDV are frequency shifted to detect possible reversed flows. The laser light source provides approximately 5-W continuous power output. The photomultiplier signal from the LDV is analyzed by counter-type signal processors. The data are digitally transferred to the core memory of a computer for storage on a disk and subsequent analysis.

Gas phase LDV measurements depend on seeding particles, which are small enough to follow the flow. The arrangement used here introduces titanium dioxide seed particle of an average size of 0.19 μm into the flow upstream of the flame. This seeding material has been previously tested by DeGroot[8] and shown to be able to follow highly turbulent flows at frequencies up to 1 kHz. The developed seeding arrangement provides dense seeding only in the vertical center plane of the combustor and therefore reduces the rate at which particles agglomerate on the optical windows.

The major focus of this investigation is on the unsteady velocity components in the flame region of the combustor, which are associated with the instability. These velocities have

Presented as Paper 88-2855 at the 24th Joint Propulsion Conference, Boston, MA, July 11-13, 1988; received Aug. 26, 1988; revision received May 22, 1989.

*Graduate Research Assistant. Member AIAA.
†Research Engineer; currently with Sverdrup Technology, Inc., Cleveland, OH.
‡Regents' Professor. Fellow AIAA.

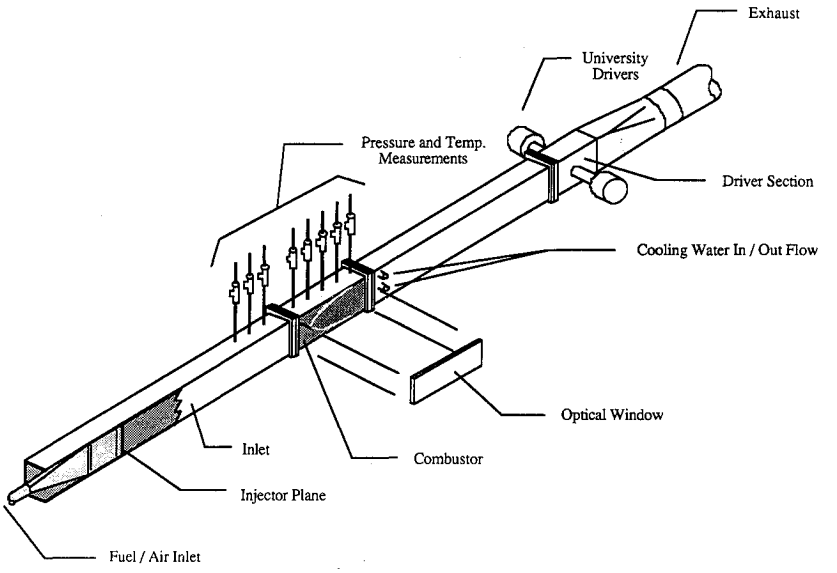

Fig. 1 Developed experimental setup.

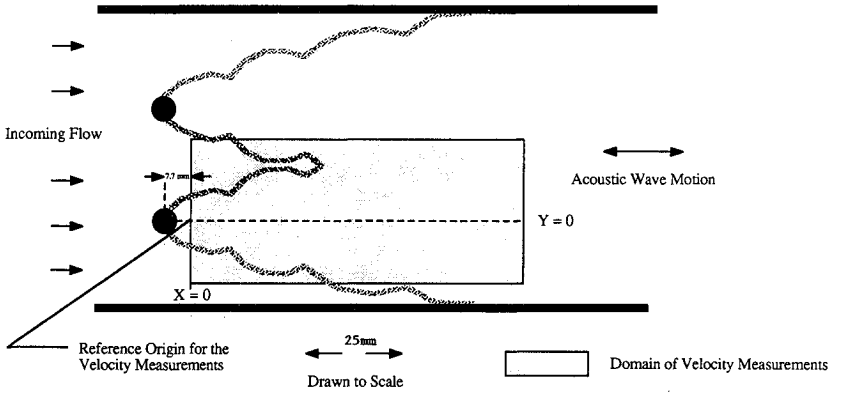

Fig. 2 Schematic of the flame geometry in the combustor.

been obtained by conditional (phase locked) sampling.[9-11] This technique determines the phase of each velocity data point with respect to a reference signal. Since the acoustic instability is expected to be synchronized with the oscillations of the velocity field, a trigger pulse generated electronically from the pressure signal has been used to start each sample period that spans one cycle of the pressure oscillation. Each sample period is divided in the present investigation into 16 subintervals, each of which may be "tagged" with the relevant phase ϕ of the pressure. Data are collected over a number of sample periods (approximately 3000 data points are typically obtained). A phase averaging technique described next is then used to obtain the steady-state and phase-dependent components of the velocity vector. The velocity vector v is written as

$$v = Ui + Vj$$

where U and V are the axial and normal components respectively. The data in each phase subinterval for each component (U or V) are first averaged. This results in 16 averaged velocity data points (for each velocity component) spanning one cycle of the pressure oscillation. A least-squares cosine curve is then employed to "fit" the measured velocity as a function of the phase angle. For example,

$$U = \bar{U} + U'$$

where

$$U' = U_0 \cos(\phi + \theta)$$

where U is the steady-state or phase-independent component of U, U_0 is the amplitude of the phase-dependent component U', and θ is the phase of U' with respect to the pressure. The component V is considered in a similar fashion so that finally,

$$V = Ui + Vj = \bar{v} + v' = (\bar{U} + U')i + (\bar{V} + V')j$$

The experimental setup is mounted on a linear, two-axis, translating system. Two stepper motors, controlled by the same host computer that collects the data from the LDV, are used to actuate each axis of the system. The experiment is moved in the X (axial) and Y (normal) coordinate directions, and the probe volume of the LDV remains stationary. The domain of the velocity measurements comprises a rectangle in a vertical plane centered between the two quartz windows of the combustor (see Fig. 2). The zero reference point is located 7.7 mm downstream of the center of the lower flame holder. The boundaries of the measured rectangular domain extend axially 90 mm downstream and from 16.5 mm below to 21.6 mm above the reference point. The measurement points are the nodes of a 26 × 21 staggered rectangular grid with a high density of points in the wake of the flame holder where the grid spacing is reduced to 1.3 mm in both axes from spacings of ΔX (in X) of 7.6 mm and a ΔY (in Y) of 2.5 mm at the upper and lower limit of the downstream boundary. It should also be noted that the vertical arrangement of the grid is not symmetric with respect to the reference origin. The grid spacing is more dense above the center line from $Y = 0$ to $Y = 10$ mm. This spacing provides more details of the flowfield in the upper half plane, and the lower points merely serve to confirm the symmetry of the shedding process.

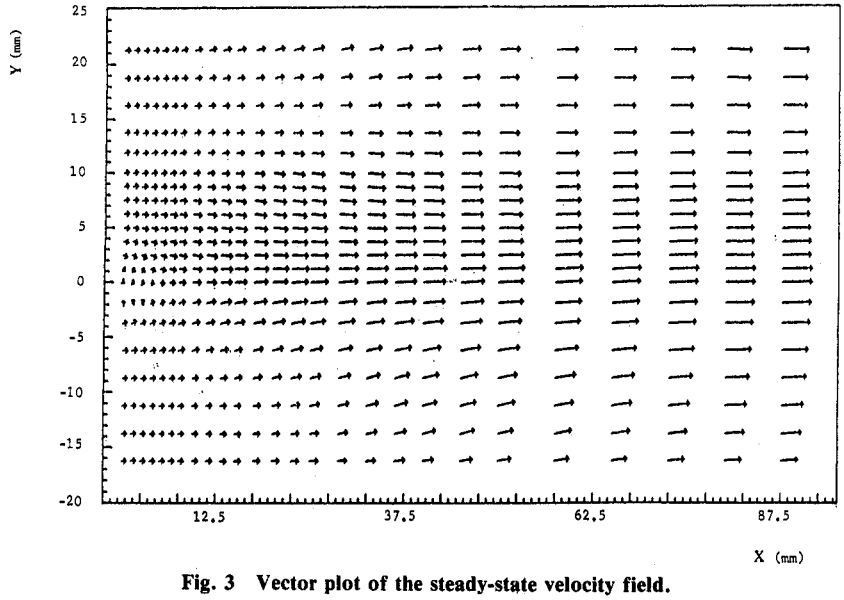

Fig. 3 Vector plot of the steady-state velocity field.

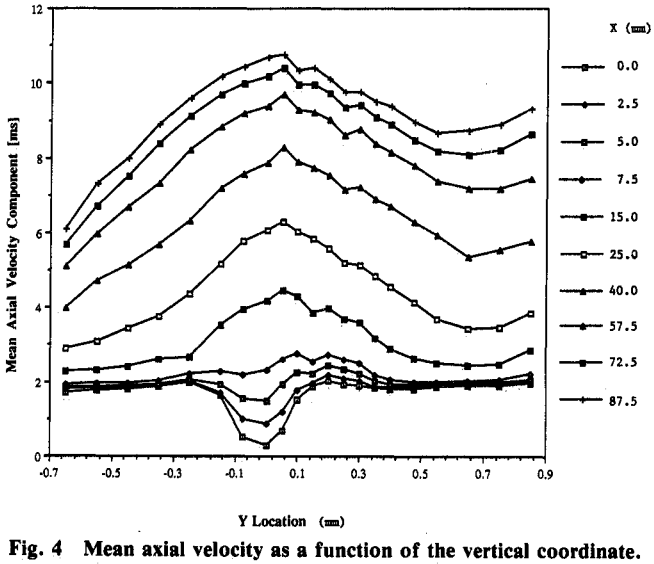

Fig. 4 Mean axial velocity as a function of the vertical coordinate.

Experimental Results

The velocity field of the W-shaped, premixed, symmetrical flame (see Fig. 2) has been measured. As noted earlier, this configuration resulted in an instability of the fundamental longitudinal mode ($f_0 = 80$ Hz) of the duct. Figure 3 shows a vector plot of the steady-state velocity field in the domain of measurement. The length of each vector scales with the magnitude of the velocity, and the orientation of the arrow shows the direction of the local flow. The mean flow accelerates from 1.9 m/s at the inflow boundary to an average of about 9.0 m/s at the outflow boundary. The velocity profile is largely parallel to the duct axis with the exception of a velocity deficit in the wake of the flame holding cylinder. The burned gas temperature has been calculated based on mass conservation of the flow in the duct, and the calculated result of 1150°C is close to the result obtained from thermocouple measurements.

The mean axial velocity profile is shown in Fig. 4 as a function of Y for several axial locations. The plot shows that the flow behind the cylinder accelerates quickly due to the decrease in density of the burned combustion products. Therefore, the velocity deficit in the wake of the cylinder disappears at about $X = 7.5$ mm and causes a reversal in the shear layer velocity gradients. The implications of this behavior will be further discussed shortly. Figure 5 shows the mean U velocity component as a function of X for several vertical Y locations. This plot also clearly shows the axial acceleration of the flow as well as the velocity deficit in the wake of the cylindrical flame holder.

The remainder of the paper focuses on the unsteady velocities and their effect on the flame structure. The phase of the pressure oscillation is denoted by ϕ. A phase of $\phi = 0$ deg represents the phase of maximum acoustic pressure during a cycle. Figure 6 superimposes the instantaneous total velocity vectors (mean plus phase-dependent components) for $\phi = 0$ deg and $\phi = 180$ deg. The velocity vectors fall very much on top of each other over much of the flow region with the exception of the wake flow behind the cylinder. This result indicates that the unsteady component of the velocity vector v' is small compared to the mean velocity vector $\bar{v}$ over most of the measurement domain. For example, at a typical location [$X = (25$ mm, -11.5 mm)] the magnitude of the mean velocity is $|\bar{v}| = 3.47$ m/s, whereas the amplitude of the unsteady velocity is $|v'| = 0.24$ m/s. It should be noted, however, that a steep increase in the standard deviation σ of the phase averaged velocity is observed as the measurements progress from the cold to the burned region of the flow. For example, typical values measured are

$X_1 = (2.5$ mm, -11.5 mm): $|\bar{v}| = 1.84$ m/s $\sigma \cong 0.25$ m/s

$X_2 = (40$ mm, -11.5 mm): $|\bar{v}| = 5.20$ m/s $\sigma \cong 1.0$ m/s

This increase in the measured standard deviation of the velocity signal is most likely due to an increased turbulence level caused by the shear flow dynamics and the combustion process as has been reported previously.[12] However, it is possible that changes in the flowfield, which are periodic at frequencies other than the frequency of instability, could also cause the observed increase in the standard deviation of the velocity signal.

The steady vorticity $\bar{\omega}$ of the flow is given by

$$\bar{\omega} = \frac{\partial \bar{V}}{\partial X} - \frac{\partial \bar{U}}{\partial Y}$$

where $\bar{U}$ and $\bar{V}$ are the steady velocity components in the X (axial) and Y (normal) directions. The steady vorticity may be experimentally determined by finite differencing the above equation using the measured steady velocity components $\bar{U}$ and $\bar{V}$. Similarly, the unsteady vorticity ω' may be calculated from the unsteady velocity components U' and V'. The steady vorticity of the flow is shown in Fig. 7. The plot shows equivorticity lines with an increment of 3 rad/s. The figure

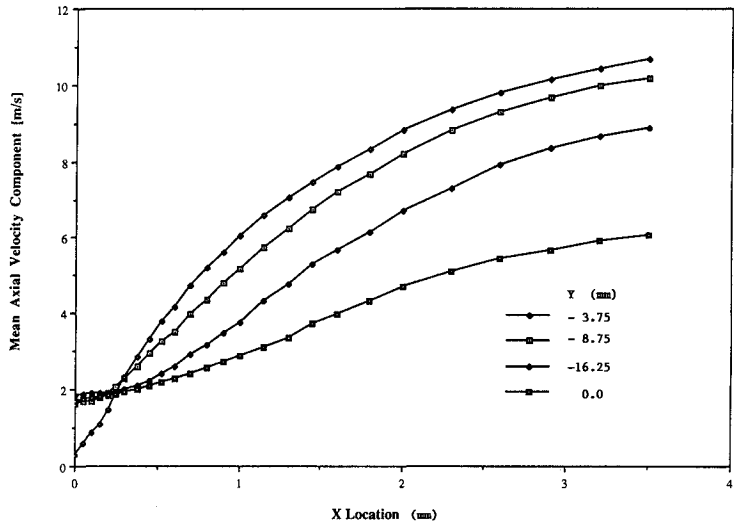

Fig. 5 Mean axial velocity as a function of the axial coordinate.

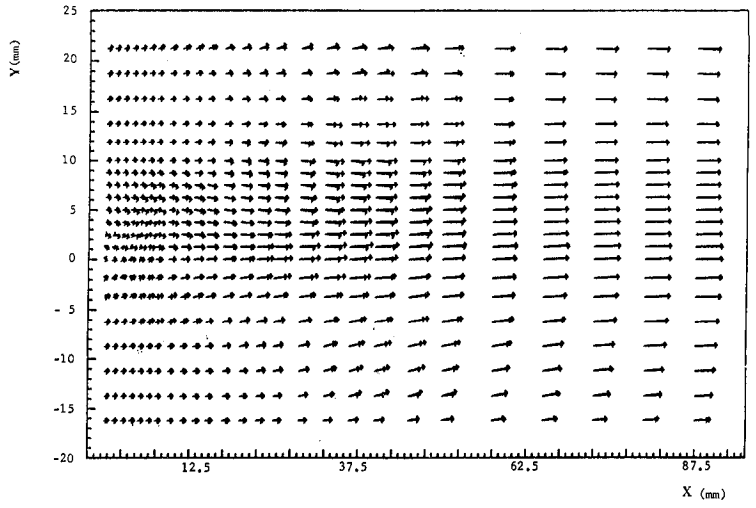

Fig. 6 Superimposed instantaneous velocity vectors at $\phi = 0$ deg and $\phi = 180$ deg.

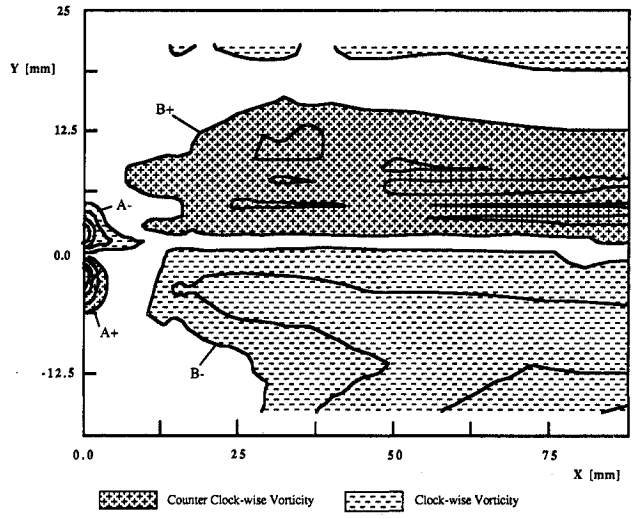

Fig. 7 Mean vorticity field.

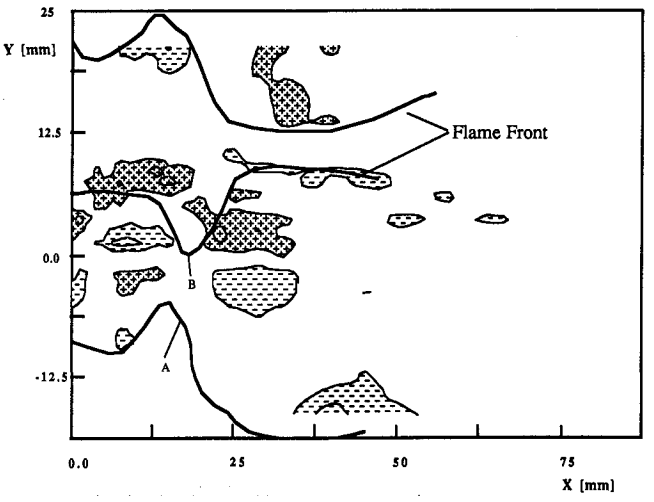

Fig. 8 Unsteady vortical field for $\phi = 0$ deg.

shows a counter-rotating vortex pair (A + and A − in Fig. 7) directly in the wake of the flame holder. This is caused by the velocity deficit of the wake. A second large pair of vortices (B + and B − in Fig. 7) is located further downstream of the first pair. This second pair has the opposite sign compared to the first pair. This behavior is a manifestation of the accelerated flow downstream of the flame holders and the resulting reversal in the shear-layer velocity gradients noted earlier in connection with Fig. 4.

Figures 8–11 show the unsteady vorticity at $\phi = 0$, 90, 180,

and 270 deg. The velocity measurements reveal pairs of counter-rotating vortices shed at the frequency of instability. During one period of the instability, two pairs of vortices of opposite sign appear in the wake on both the top and bottom surfaces of the flame holder. As these vortices are accelerated by the mean flowfield, they also undergo stretching and lose intensity. The convection velocity of the structures is estimated as 1 ± 0.5 m/s at $X = 5$ mm and 4 ± 0.5 m/s at $X = 25$ mm. These values correspond approximately to the average velocities at these locations as may be observed from Fig. 4. Hence, these results confirm that the unsteady vortical structures are convected with approximately the local mean-flow velocity as suggested by earlier studies.[1]

Figures 8-11 also show the instantaneous flame front superimposed on the unsteady vorticity. The location of the flame front has been obtained by means of a phase-locked shadow photography technique described elsewhere.[13] Note that the scale of the abscissa differs from the scale of the ordinate, and therefore the flame shape and the thickness of the vortices are distorted. These figures suggest that the unsteady vortices cause the flame-front perturbations, which are observed in the shadowgraph pictures. For example, at $\phi = 0$ deg, the "kinks" at $X = 17.5$ mm in the flame (branch A and B in Fig. 8) are believed to be caused by the adjacent counter rotating vortex pair. The "kinks" (branch A and B in Fig. 9 at $X = 17.5$ mm) continue to grow in size, and the flame fronts are simultaneously rolled up by vortical structures marked A + and B − . As the reaction fronts move closer together, all the reactants between the two fronts are consumed and the kinks collapse, as evident from Fig. 10 where the remainder of the kinks are labeled A and B. The process repeats itself in a new cycle. For example, the first occurrence of flame perturbations are marked C and D at the inflow boundary of Fig. 11. Therefore, it is evident that the vortex shedding causes a periodic distortion of the flame front.

The distortion of the flame front results in a cyclic variation of the flame area.[2] Because the reactants are consumed at the flame surface, the instantaneous flame surface area (the flame length in the two-dimensional approximation) is a measure of the instantaneous reaction rate and, hence, the instantaneous heat release rate. The flame length has been determined experimentally as a function of the phase of the pressure oscillation by means of shadow photography.[13] The measured variation in flame length is shown in Fig. 12 together with the acoustic pressure levels as a function of the phase of the pressure oscillation. The flame length is seen to be approximately in phase with the pressure, which is measured here by a wall-mounted pressure transducer at the flame holder location. It should be noted that the pressure oscillation is, to a very good approximation, constant over the length of the flame. The reason for this is that the flame length is much smaller than the acoustic wavelength at the frequency f_0. This finding suggests that the unsteady combustion and heat release rates are in phase with the pressure. It should be noted that this is consistent with Rayleigh's criterion[14] for the driving of acoustic waves by heat addition (i.e., the flame). Hence, the obtained flowfield measurements demonstrate that the vortex shedding at the flame holder results in an unsteady heat release rate capable of driving the observed combustion instability in the burner.

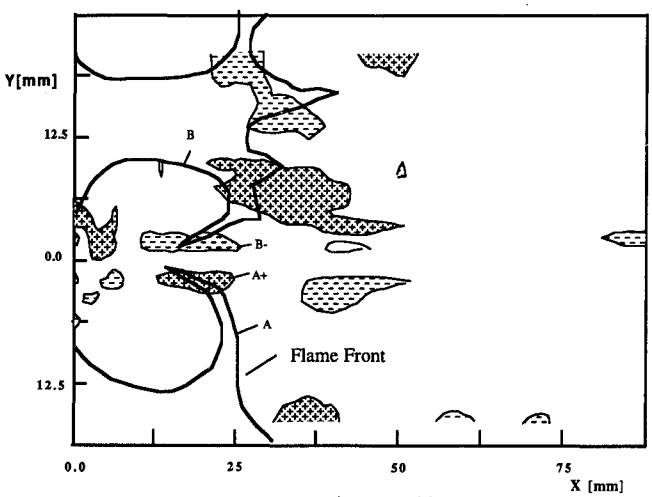

Fig. 9 Unsteady vortical field for $\phi = 90$ deg.

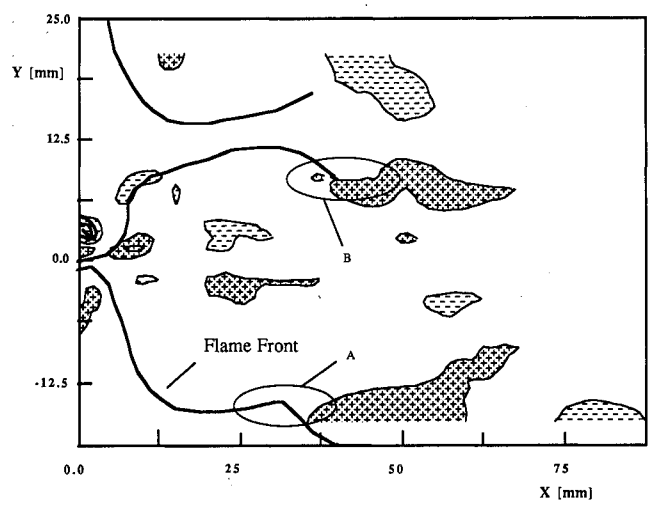

Fig. 10 Unsteady vortical field for $\phi = 180$ deg.

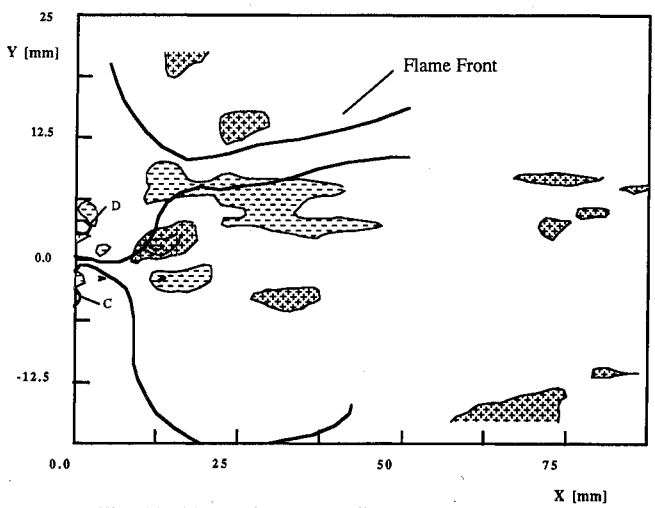

Fig. 11 Unsteady vortical field for $\phi = 270$ deg.

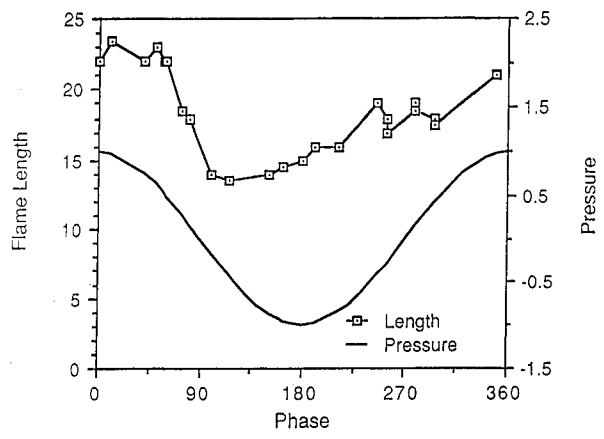

Fig. 12 Flame length and pressure as functions of the phase of the pressure.

Conclusions

The role of the fluid mechanics of the flame region on the driving of combustion instabilities in a ramjet engine has been studied. Extensive measurements of the unsteady flowfield have been carried out to characterize the interaction between the ramjet flame and the unsteady vortical field downstream of the flame holders. These measurements show that symmetric and periodic vortex shedding occurs in the wake of the flame holder at the frequency of instability. These vortices, in turn, periodically distort the flame front and cause oscillatory changes in the heat release rate, which are capable of driving the observed instabilities.

Acknowledgment

This work has been supported by the Office of Naval Research under Contract N00014-84-K-0470.

References

[1]Hegde, U. G., Reuter, D., Daniel, B. R., and Zinn, B. T., "Flame Driving of Longitudinal Instabilities in Dump Type Ramjet Combustors," *Combustion Science and Technology*, Vol. 55, No. 4-6, p. 125.

[2]Hegde, U. G., Reuter, D., and Zinn, B. T., "Combustion Instability Mechanisms in Ramjets," AIAA Paper 88-0150, Jan. 1988.

[3]Kailasanath, K., Gardner, J. H., Boris, J. P., and Oran, E., "Interactions Between Acoustics and Vortex Structures in a Central Dump Combustor," AIAA Paper 86-1609, June 1986.

[4]Sterling, J. D., and Zukoski, E. E., "Longitudinal Mode Combustion Instabilities in a Dump Combustor," AIAA Paper 87-0220, Jan. 1987.

[5]Schadow, K. C., Gutmark, E., Parr, T. P., Parr, D. M., and Wilson, K. H., "Passive Shear-Flow Control to Minimize Ramjet Combustion Instability," *Proceedings of the 23rd JANNAF Combustion Meeting*, Chemical Propulsion Information Agency, Applied Physics Lab., Laurel, MD, Oct. 1986.

[6]Flandro, G. A., and Finlayson, P. A., "Nonlinear Interactions Between Vortices and Acoustic Waves in a Rocket Combustion Chamber," *21st JANNAF Combustion Meeting*, Chemical Propulsion Information Agency, Applied Physics Lab., Laurel, MD, Oct. 1984.

[7]Smith, D. A., and Zukoski, E. E., "Combustion Instability Sustained by Unsteady Vortex Combustion," AIAA Paper 85-1248, July 1985.

[8]DeGroot, W. A., "Laser Diagnostics of the Flow Behind a Backward Facing Step," Ph.D. Thesis, Georgia Inst. of Technology, Atlanta, GA, 1985.

[9]Bell, W. A., and Lepicovsky, J., "Conditional Sampling with a Laser Velocimeter," AIAA Paper 83-0756, Jan. 1983.

[10]Sankar, S. V., "Investigation of the Flame-Acoustic Wave Interaction During Axial Solid Rocket Instabilities," Ph.D. Thesis, Georgia Inst. of Technology, Atlanta, GA, 1987.

[11]Lepicovsky, J., "Laser Velocimeter Measurements of Large-Scale Structures in a Tone-Excited Jet," *AIAA Journal*, Vol. 24, No. 1, pp. 27-31, 1986.

[12]Ballal, D. R., and Chen, T.-H., "Turbulence-Combustion Interaction in Practical Combustion Systems," AIAA Paper 86-1607, July 1986.

[13]Hedge, U. G., Reuter, D., and Zinn, B. T., "Driving Mechanisms in Unstable Ramjet Combustors," *16th ICAS Congress*, AIAA, Washington, DC, Aug. 1988.

[14]Lord Rayleigh, *The Theory of Sound,* Vol. II, Dover, New York, 1945, pp. 224-235.